



## Co<sub>0.56</sub>Ni<sub>0.44</sub> Oxide Nanoflake Materials and Activated Carbon for Asymmetric Supercapacitor

Jun-Wei Lang,<sup>a</sup> Ling-Bin Kong,<sup>a,b,z</sup> Min Liu,<sup>a</sup> Yong-Chun Luo,<sup>b</sup> and Long Kang<sup>b</sup>

<sup>a</sup>State Key Laboratory of Gansu Advanced Non-ferrous Metal Materials and <sup>b</sup>School of Materials Science and Engineering, Lanzhou University of Technology, Lanzhou 730050, People's Republic of China

In this work, Co<sub>0.56</sub>Ni<sub>0.44</sub> oxide nanoflakes with a maximum specific capacitance of 1227 F/g (136 mAh/g) are successfully synthesized by a facile chemical coprecipitation method. To enhance energy density, an asymmetric supercapacitor with high energy and power density has been constructed with Co<sub>0.56</sub>Ni<sub>0.44</sub> oxide nanoflakes as the positive electrode and activated carbon as the negative electrode. The performance of the asymmetric supercapacitor was characterized by cyclic voltammetry and chronopotentiometry technology. By using the nanoflakes Co<sub>0.56</sub>Ni<sub>0.44</sub> oxides electrode, the asymmetric supercapacitor exhibits high energy density and stable power characteristics; the maximum specific capacitance of 97 F/g and specific energy of 34.5 W h/kg are demonstrated for a cell voltage between 0 and 1.6 V.

© 2010 The Electrochemical Society. [DOI: 10.1149/1.3497298] All rights reserved.

Manuscript submitted May 24, 2010; revised manuscript received August 12, 2010. Published October 16, 2010.

Supercapacitors provide a higher energy density than dielectric capacitors and a higher power density than batteries. They are particularly adapted for applications which require energy pulses during short periods of time.<sup>1-3</sup> However, for the electrochemical double-layer capacitors (EDLCs) and most pseudocapacitors, the specific energy of electrochemical capacitors is still much less than that of advance batteries.<sup>4-6</sup> Therefore, in order to satisfy the industrial demand, the development of new materials and new concepts for supercapacitors should be proposed.

In its charged state, a supercapacitor is equivalent to two electrodes of capacitances  $C_1$  and  $C_2$  in series. As the capacity of the two electrodes is different, even in a symmetric capacitor, the capacity of the total system  $C$  is determined by the electrode with the smaller capacity value. Moreover, the later electrode operates in a larger potential window than the other one, what consequently reduces the voltage range of the device. This drawback can be circumvented by balancing the respective masses of the electrodes or by using different materials working in their optimal potential range.<sup>7,8</sup> The asymmetric design is an attractive approach to increasing the energy density of supercapacitors as it can lead to an almost doubling of device capacitance.

For the asymmetric supercapacitor, a new concept of high energy density electrochemical capacitor, one electrode stores charge through a reversible, nonfaradaic reaction of ion adsorption/desorption on the surface of the an activated carbon (AC), and the other electrode is to utilize a reversible redox faradaic reaction in a transition metal oxide. It is possible to reach the high working voltage and high energy density by choosing a proper electrode material, contributed to a significant increase in the overall energy density of the supercapacitor devices.<sup>9-11</sup>

Supercapacitors make use of three main classes of materials: carbon,<sup>12-15</sup> metal oxide,<sup>16-19</sup> and electronically conducting polymer.<sup>20-22</sup> Among these electrode materials, AC, as the representative electrode material of the EDLCs, has rapid current-voltage ( $I$ - $V$ ) response and rectangle cyclic voltammetry (CV) shape, whereas its specific capacitance is relatively low.<sup>23</sup> Electroactive materials with several oxidation states or structures, such as transition metal oxides and conducting polymers, can provide a large reversible capacity, good cycling performance, and high recharging rates for pseudocapacitors.<sup>24-28</sup> Conducting-polymer capacitors have been reported to display high power densities, but their specific capacitances are much lower than those of metal oxide capacitors. Hence, it would be of great interest to develop a metal oxides electrode material with the large capacity and high rate capability for supercapacitors.

The natural abundance and low cost of nickel oxide, accompa-

nied by its energy storage performance in basic electrolytes and environment compatibility, have made it one of the most promising electrode materials for pseudocapacitors.<sup>29</sup> However, issues related to its electrochemical characteristics, such as conductivity and the utilization of the active material, still remain unresolved.<sup>30</sup> In order to improve the nickel oxide performance, great efforts have been made. In fact, cobalt compounds are also studied as cheaper candidates with good capacitive characteristics due to its many important technological applications. Moreover, cobalt compounds are potentially good additions for improving the properties of the nickel electrode in the nickel-metal hydride (Ni/MH) battery.<sup>31,32</sup> Adding cobalt compounds can significantly enhance nickel oxide utilization as cobalt can reduce the resistance of the nickel electrode and raise the oxygen overpotential.<sup>33-35</sup>

In this work, nickel-cobalt oxide nanoflakes were successfully synthesized by a facile chemical coprecipitation method followed by a simple calcinations process. The studies show that the composites nickel-cobalt oxides nanoflakes with less crystallization were composed of NiO and Co<sub>3</sub>O<sub>4</sub>. The maximum specific capacitance of 1227 F/g (136 mAh/g) is the highest report of nickel-cobalt oxides for electrochemical capacitors, which shows better rate capability and great potential as the electrode materials for electrochemical capacitors. To enhance energy density, an asymmetric-type pseudocapacitor/electric double-layer capacitor is considered, where Co<sub>0.56</sub>Ni<sub>0.44</sub> oxide nanoflakes and activated carbon act as the positive and negative electrodes, respectively. Electrochemical measurements were carried out in 2 M aqueous KOH in a half-cell setup configuration at room temperature using CV, chronopotentiometry, and impedance spectroscopy. Values for the maximum specific capacitance and specific energy of 97 F/g and 34.5 W h/kg, respectively, are demonstrated for a cell voltage between 0 and 1.6 V. By using the nanoflakes Co<sub>0.56</sub>Ni<sub>0.44</sub> oxide electrode, the asymmetric supercapacitor exhibits high energy density and excellent power characteristics.

### Experimental

*Preparation of the electrode material.*—All of the chemicals were of analytical grade and were used without further purification. Co<sub>0.56</sub>Ni<sub>0.44</sub> oxides were synthesized by a facile chemical coprecipitation method followed by a simple calcinations process. First, a mixed aqueous solution of 1 M NiCl<sub>2</sub>·6H<sub>2</sub>O and 1 M CoCl<sub>2</sub>·6H<sub>2</sub>O was made, the molar ratios of the CoCl<sub>2</sub>·6H<sub>2</sub>O:NiCl<sub>2</sub>·6H<sub>2</sub>O was 1:3. The pH value of the mixed solution was slowly adjusted to 9 by adding slowly 5 wt % NH<sub>3</sub>·H<sub>2</sub>O at room temperature. The resulting suspension was kept stirring at this temperature for 3 h. Then the solid was filtered, washed with distilled water several times, and dried in air at 250°C for 6 h.

Commercial AC (The ShaoWu XinSen Carbon Company, China,

<sup>z</sup> E-mail: konglb@lut.cn

with a specific surface area of 2000 m<sup>2</sup>/g and a diameter of 5–10 μm) was used as the negative electrode material without further treatment.

**Structure characterization.**—The obtained products were characterized by field emission scanning electron microscope (SEM) (JEOL, JSM-6701F, Japan), X-ray diffraction (XRD) measurements (Rigaku, D/Max-2400, Japan), and nitrogen adsorption and desorption experiments (Micromeritics, ASAP 2020M, USA). The surface area was calculated using the Brunauer–Emmett–Teller (BET) equation. Pore-size distributions were calculated by the Barrett–Joyner–Halenda (BJH) method using the desorption branch of the isotherm. The elemental composition in the as-prepared samples was determined using the energy dispersive spectrum (EDS) coupled to the SEM instrument.

**Preparation of the electrode.**—The working electrodes were prepared according to the method reported in Ref. 1. Nickel–cobalt oxide powder (80 wt %) was mixed with 7.5 wt % of acetylene black (> 99.9%) and 7.5 wt % of conducting graphite in an agate mortar, until a homogeneous black powder was obtained. To this mixture, 5 wt % of poly(tetrafluoroethylene) was added with a few drops of ethanol. After briefly allowing the solvent to evaporate, the resulting paste was pressed at 10 MPa to a nickel gauze with a nickel wire for an electric connection. The electrode assembly was dried for 16 h at 80°C in air. The AC electrodes were prepared by the same method as the negative electrode described above.

**Electrochemical test of the single electrode and asymmetric supercapacitor.**—The electrochemical measurements of single nickel–cobalt oxide and AC electrodes were carried out using an electrochemical working station (CHI660C, Shanghai, China) in a three-electrode cell at room temperature. A platinum gauze electrode and a saturated calomel electrode (SCE) served as the counter electrode and the reference electrode, respectively. Each electrode contained about 8 mg of electroactive material and had a geometric surface area of about 1 cm<sup>2</sup>.

The nickel–cobalt oxide cathode and AC anode were pressed together and separated by a porous nonwoven cloth separator. The mass ratio of active materials (anode/cathode) was 22:8 mg. Each electrode had a geometric surface area of about 1 cm<sup>2</sup>. The electrochemical measurements of the asymmetric supercapacitor were also carried out using the electrochemical working station in a two-electrode cell at room temperature.

The specific capacitance of the asymmetric capacitor can be evaluated from the charge/discharge test together with the following equation

$$C = I[(dE/dt) \times m] \approx I[(\Delta E/\Delta t) \times m] \text{ (F/g)} \quad [1]$$

where  $C$  is the specific capacitance,  $I$  is the constant discharging current,  $\Delta t$  is the time period for the potential change  $\Delta E$ , and  $m$  is the mass of the corresponding electrode materials measured.

The charge on the electrode can be evaluated from the charge/discharge test together with the following equation

$$C' = I\Delta t/m \text{ (C/g)} \quad [2]$$

where  $I$  is the constant discharging current,  $\Delta t$  is the time period for the potential change, and  $m$  is the mass of the corresponding electrode materials measured.

The real power density  $P_{\text{real}}$  is determined from the constant current charge/discharge cycles as follows<sup>36</sup>

$$P_{\text{real}} = \Delta E I/m \text{ (W/kg)} \quad [3]$$

where  $\Delta E = (E_{\text{max}} + E_{\text{min}})/2$  with  $E_{\text{max}}$  being the potential at the end of the charge and  $E_{\text{min}}$  being the potential at the end of the discharge,  $E_{\text{min}}$  is the applied current (amperes), and  $m$  is the weight of active material in the electrode (kilograms).

The specific energy  $E_{\text{real}}$  is defined as

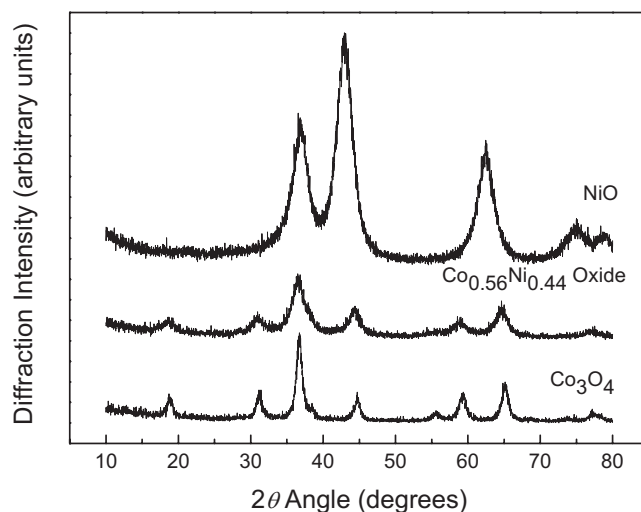


**Figure 1.** The XRD patterns of the nickel oxide, Co<sub>0.56</sub>Ni<sub>0.44</sub> oxide, and cobalt oxide.

$$E = CU_{\text{max}}^2/2 \text{ (W h/kg)} \quad [4]$$

where  $C$  is the system capacitance for a cell and  $U_{\text{max}}$  is the maximum cell voltage.

## Results and Discussion

**Characterization of Co<sub>0.56</sub>Ni<sub>0.44</sub> oxide materials.**—The atomic percentages (atom %) of the elements Co and Ni in nickel–cobalt oxides were obtained by means of EDS spectroscopy. The result shows that the Co<sub>0.56</sub>Ni<sub>0.44</sub> oxide material is obtained when the molar ratio of the CoCl<sub>2</sub>·6H<sub>2</sub>O:NiCl<sub>2</sub>·6H<sub>2</sub>O in mixed solution was 1:3.

The XRD patterns of the nickel oxide, Co<sub>0.56</sub>Ni<sub>0.44</sub> oxide, and cobalt oxide are shown in Fig. 1. All the diffraction peaks of pure nickel oxide sample, including not only the peak positions but also their relative intensities, are in good accordance with the cubic crystalline structure of NiO (Powder Diffraction File (PDF), no. 22-1189). All diffraction peaks of the cobalt oxides sample are in good accordance with the diffraction data of the spinel structure Co<sub>3</sub>O<sub>4</sub> (PDF, no. 42-1467). It is obvious that the Co<sub>0.56</sub>Ni<sub>0.44</sub> oxide is composed of NiO and Co<sub>3</sub>O<sub>4</sub>. It is difficult to differentiate between the two phases, since they have similar structures and their diffraction peaks are very close. The peaks of the Co<sub>0.56</sub>Ni<sub>0.44</sub> oxide are broad, which indicates the low degree of crystallization of the products; the crystallite size of the Co<sub>0.56</sub>Ni<sub>0.44</sub> oxide was 44.6 Å which was calculated from the Scherrer formula.

SEM measurement was performed to the Co<sub>0.56</sub>Ni<sub>0.44</sub> oxide. As seen in Fig. 2, the Co<sub>0.56</sub>Ni<sub>0.44</sub> oxide has a spherical morphology with 2–3 μm diameter, which is built up of many interleaving thin nanoflakes. It can be observed that the Co<sub>0.56</sub>Ni<sub>0.44</sub> oxide possesses many macropores that are hundreds of nanometers in size on the surface.

Surface area and pore-size distribution analysis of the Co<sub>0.56</sub>Ni<sub>0.44</sub> oxide materials were conducted using N<sub>2</sub> adsorption and desorption experiments. As shown in Fig. 3, the profile of the hysteresis loop indicates an adsorption–desorption characteristic of the porous materials. The BET specific surface area of the Co<sub>0.56</sub>Ni<sub>0.44</sub> oxide was 110 m<sup>2</sup>/g. The inset is the pore diameter distributions of the Co<sub>0.56</sub>Ni<sub>0.44</sub> oxide sample. As shown in this figure, the Co<sub>0.56</sub>Ni<sub>0.44</sub> oxides possess a narrow mesoporous distribution at around 2–7 nm. The BJH desorption average pore diameter for the Co<sub>0.56</sub>Ni<sub>0.44</sub> oxide was 5.9 nm.

**The electrochemical characterizations of the Co<sub>0.56</sub>Ni<sub>0.44</sub> oxide material and AC electrodes.**—To evaluate the electrochemical properties of the prepared Co<sub>0.56</sub>Ni<sub>0.44</sub> oxides material and the com-

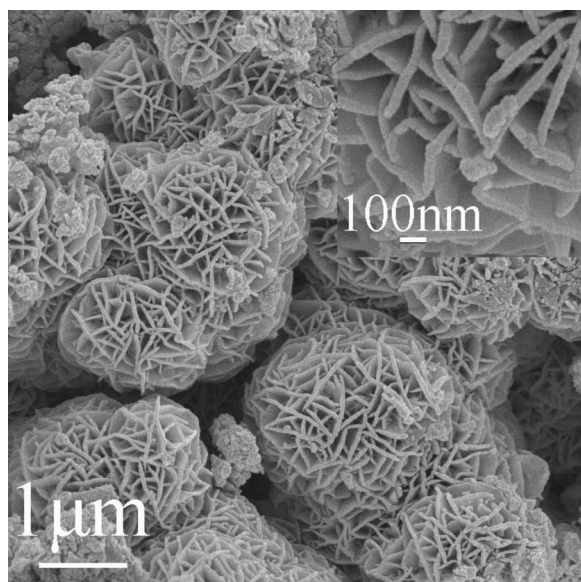


**Figure 2.** SEM images of the  $\text{Co}_{0.56}\text{Ni}_{0.44}$  oxide material.

mercial AC, we directly use these two materials to fabricate electrodes for supercapacitors. CV and chronopotentiometry measurements have been used to evaluate the electrochemical properties and quantify the specific capacitance of the  $\text{Co}_{0.56}\text{Ni}_{0.44}$  oxides and AC electrodes. CV curves for AC and  $\text{Co}_{0.56}\text{Ni}_{0.44}$  oxides electrodes in 2 M KOH aqueous solution are shown in Fig. 4. The AC electrode was performed within a potential window of  $-1.0$  to  $0$  V (versus SCE), and  $\text{Co}_{0.56}\text{Ni}_{0.44}$  oxides was employed within a potential window of  $0$ – $0.5$  V (versus SCE) at a scan rate of  $5$  mV/s. For the AC electrode, a nearly rectangular CV curve is obtained, indicating a typical e EDLC behavior because no peaks of oxidation and reduction are observed. The CV shapes of  $\text{Co}_{0.56}\text{Ni}_{0.44}$  oxides reveal that the capacitance characteristic is very distinguished from that of the electric double-layer capacitance. Obviously, electrochemical polarization of electrodes does not appear from CV curves at the two edges of potential window, which indicates that electrochemical capacitors with wider potential window can be chosen.

Figure 5a shows the typical galvanostatic charge/discharge curves of the  $\text{Co}_{0.56}\text{Ni}_{0.44}$  oxides electrode within a potential win-

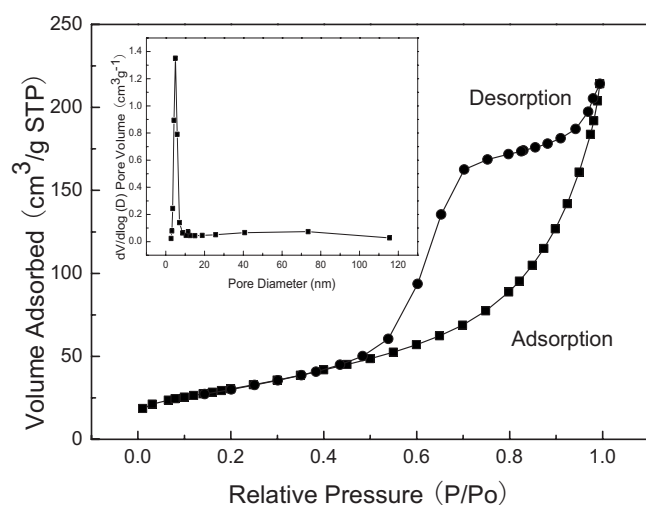


**Figure 3.** The  $\text{N}_2$  adsorption–desorption isotherm of  $\text{Co}_{0.56}\text{Ni}_{0.44}$  oxide materials; the inset is the BJH pore-size distributions of  $\text{Co}_{0.56}\text{Ni}_{0.44}$  oxide materials.

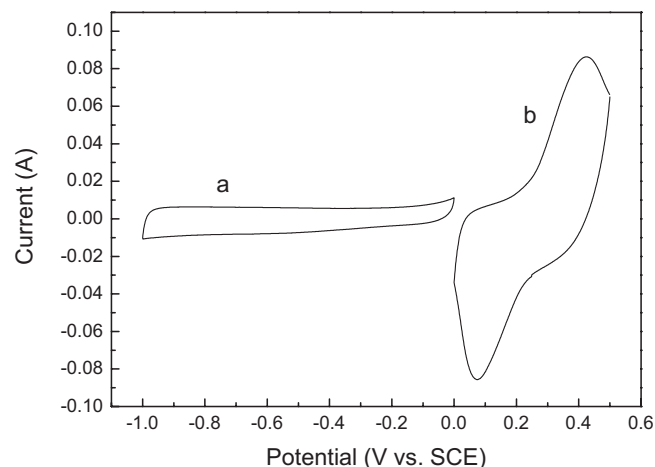


**Figure 4.** Cyclic voltammogram of (a) AC and (b)  $\text{Co}_{0.56}\text{Ni}_{0.44}$  oxide electrodes at a scan rate of  $5$  mV/s in  $2$  M KOH solution.

dow of  $0$ – $0.4$  V at a current density of  $625$  mA/g. The shape of the discharge curves does not show the characteristic of a pure double-layer capacitor, but mainly pseudocapacitance, which agrees with

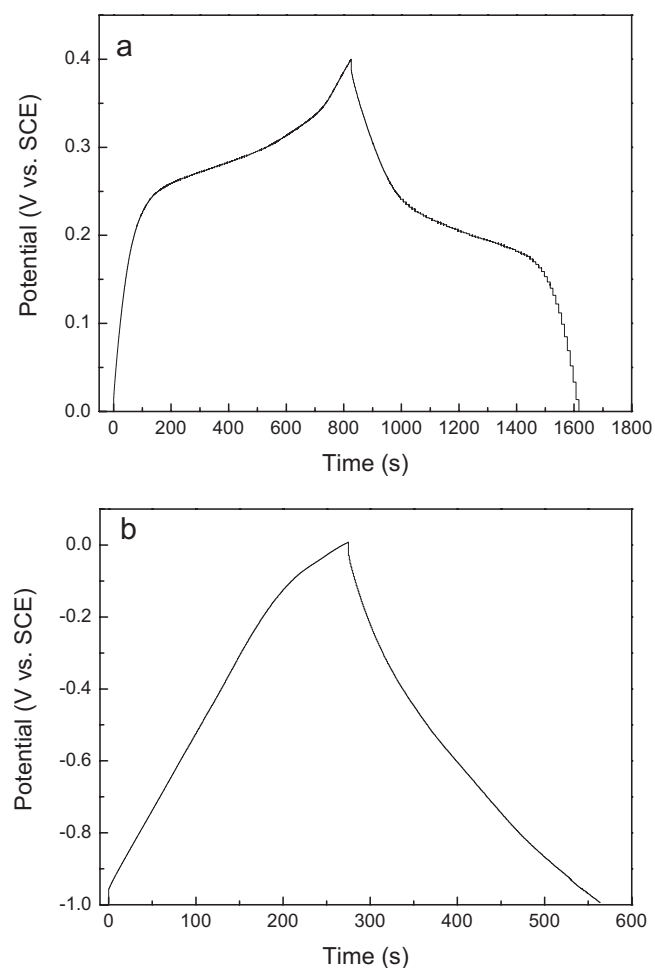


**Figure 5.** Charge/discharge curves of the (a)  $\text{Co}_{0.56}\text{Ni}_{0.44}$  oxide electrode in the potential window  $0$  to  $0.4$  V and (b) AC electrode in the potential window of  $-1$  to  $0$  V at a current density of  $625$  mA/g in  $2$  M KOH solution. Each electrode contained about  $8$  mg of electroactive material and had a geometric surface area of about  $1$   $\text{cm}^2$ .

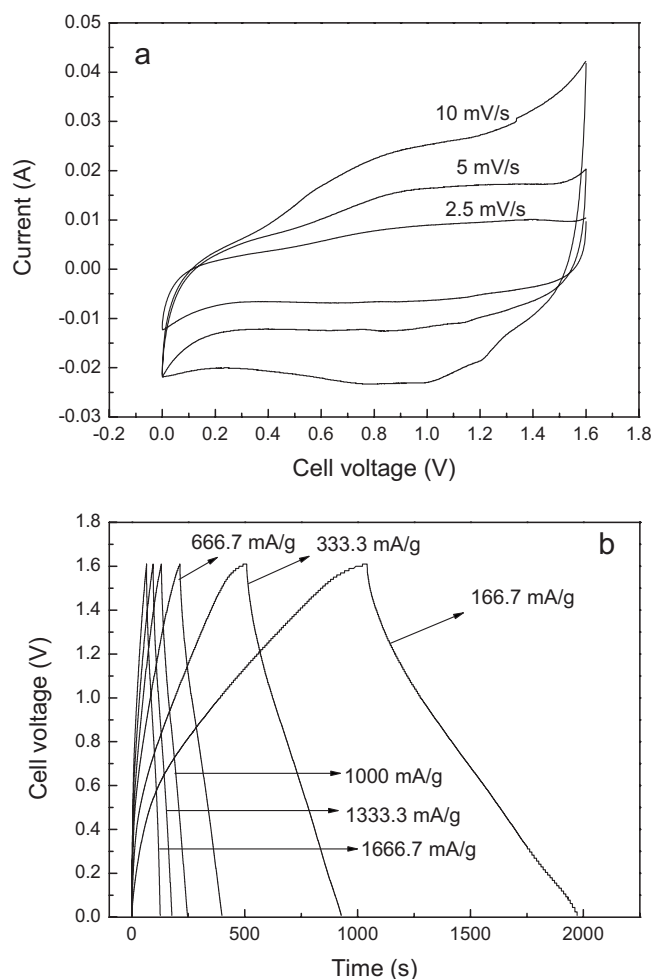


**Figure 6.** Electrochemical properties of the asymmetric supercapacitor in 2 M KOH solution within a cell voltage range from 0.0 to 1.6 V: (a) cyclic voltammograms at different scan rates and (b) charge/discharge behavior at different current densities. The mass loads of the cathode  $\text{Co}_{0.56}\text{Ni}_{0.44}$  oxide electrode material are 8 and 22 mg of the AC anode electrode material.

the result of the CV curves. The slope of charge/discharge curves indicates the potential dependent nature of the faradaic reaction. The specific capacitance value of the  $\text{Co}_{0.56}\text{Ni}_{0.44}$  oxide is calculated to be 1227 F/g (136 mAh/g), according to Eq. 1. Since the size range of the hydrated ions in the electrolyte is typically 6–7.6 Å, the pore size at the range of 8–50 Å is the effective one required to increase either the pseudocapacitance or electric double-layer capacitance.<sup>37</sup> Furthermore, the unique microstructure of the  $\text{Co}_{0.56}\text{Ni}_{0.44}$  oxides can accommodate the electroactive species in the solid bulk electrode material. Therefore, the obtained high specific capacitance of 1227 F/g from the synthesized  $\text{Co}_{0.56}\text{Ni}_{0.44}$  oxides materials is mainly attributed to the effective distributions of the pore size and the high specific surface area.

The linear charge/discharge curves are observed in Fig. 5b of the AC electrode within a potential window of –1 to 0 V at a current density of 625 mA/g. The linear shape of the curve is attributed to the linear correlation of the absorbed charge on the interface with the applied potential. That means the specific capacitance is independent of the applied potential nature, distinctly accompanied with a nonfaradaic process on the interface. The charge on the  $\text{Co}_{0.56}\text{Ni}_{0.44}$  oxide electrode and the usual AC electrode in their own potential window is 490 and 176 C/g, respectively, according to Eq. 2. Therefore, the optimal mass ratio of the  $\text{Co}_{0.56}\text{Ni}_{0.44}$  oxide elec-

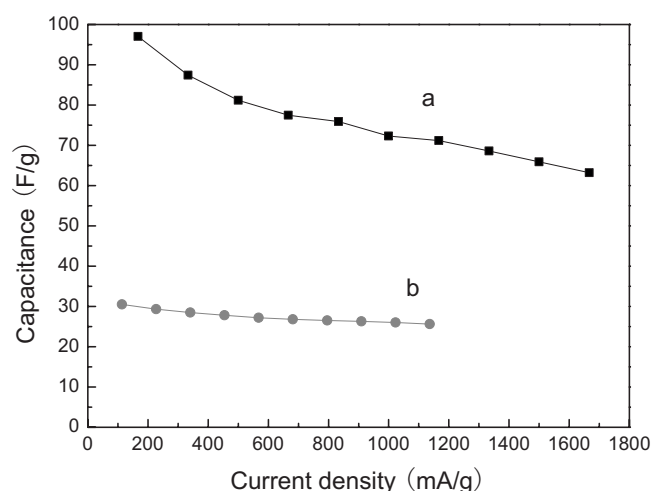


**Figure 7.** Specific capacitance as a function of discharge currents for (a) asymmetric supercapacitor and (b) AC-based EDLC capacitor.

trode and the AC electrode is 176:490, and the loads of the cathode  $\text{Co}_{0.56}\text{Ni}_{0.44}$  oxide electrode and the AC anode electrode materials are of 8 and 22 mg, respectively.

*The electrochemical characterizations of the asymmetric capacitors.*— It is very important to polarize each electrode at the same potential before cycling the device; otherwise, there is a risk of damaging the cell during the first cycles. The typical CV of the asymmetric capacitor at voltage scan rates of 2.5, 5, and 10 mV/s is depicted in Fig. 6a. The hybrid device was cycled between 0 and 1.6 V with a good reversibility in this cell voltage window. It should be noted that the CV curves can be approximately considered as rectangle shapes when the scan rate is 2.5 mV/s; when the scan rate increases to 5 mV/s, the curve begins to deform. Also, the current increases with scan rate, indicating rapid  $I$ – $V$  response.

Galvanostatic constant current charge/discharge measurements at different current densities were applied to evaluate the electrochemical properties and to quantify the specific capacitance of the asymmetric supercapacitor in 2 M KOH electrolyte. Figure 6b shows the typical galvanostatic charge–discharge curves of the hybrid capacitor between 0 and 1.6 V at different current densities. As shown in Fig. 6b, during the charging and discharging steps, though an almost linear variation in the cell voltage is observed in the curves, perfect linear curves are not obtained compared with EDLC. This is due to a typical pseudocapacitance behavior resulting from the electrochemical adsorption/absorption or redox reactions at interfaces between electrodes and electrolyte.<sup>36</sup> On account that the real galvanostatic discharge window of the  $\text{Co}_{0.56}\text{Ni}_{0.44}$  oxide electrode is about 0.5 V, the result of the present work shows that it is possible to reach the high working voltage by choosing a proper electrode material. All these profit from using the active carbon as the negative electrode materials with large surface and proper pore distribution, which ensure that the  $\text{Co}_{0.56}\text{Ni}_{0.44}$  oxides precede with the faradaic reaction in the larger applied potential range. Furthermore, as the discharge current increases, the large voltage drop is produced and finally the capacity decreases. This phenomenon may be explained by referring to  $\text{OH}^-$  ions diffusion processes during the charging/discharging for the electrode. When the electrode at high sweep rates corresponds to a high current density, massive  $\text{OH}^-$  ions are required to intercalate swiftly at the interface of the electrode/electrolyte. However, relatively low concentration of  $\text{OH}^-$  ions could not meet this demand and the processes would be controlled by the ion diffusion.<sup>38</sup>

In comparison with the asymmetric capacitor, we fabricate a two-electrode AC symmetric capacitor and it is cycled galvanostatically between 0 and 1.0 V. Each electrode contained about 22 mg of AC

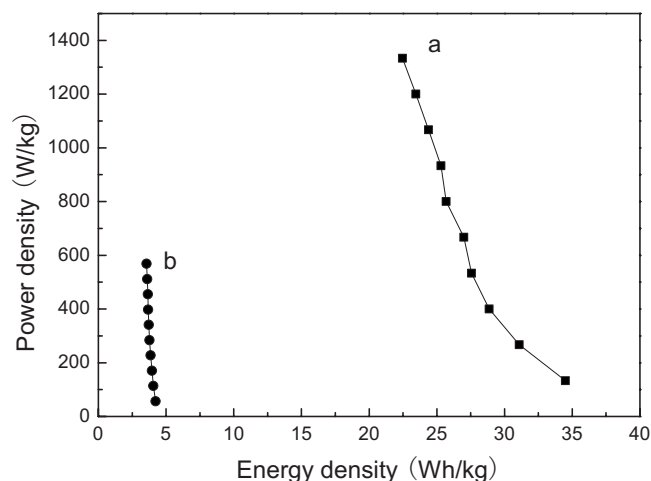


**Figure 8.** Ragone plot relating power density to achievable energy density of (a) asymmetric supercapacitor and (b) AC-based EDLC capacitor.

material and had a geometric surface area of about  $1 \text{ cm}^2$ . Figure 7 shows the specific capacitance of the double electrode cell as a function of the discharge current density for the  $\text{Co}_{0.56}\text{Ni}_{0.44}$  oxide electrode-based asymmetric supercapacitor and the AC-based EDLC. The specific capacitances (calculated based on the total weight of the active materials in the supercapacitor) of the hybrid capacitor at 166.7, 333.3, 666.7, 1000, 1333.3, and 1666.7 mA/g were 97, 87.4, 77.5, 72.3, 68.6, and 63.2 F/g, respectively. The specific capacitances of the EDLC of the total weight of the active material for both electrodes at 113.6, 227.3, 454.5, 681.8, 909.1, and 1136.4 mA/g were 30.5, 29.3, 27.8, 26.8, 26.3, and 25.6 F/g, respectively. The results show that the specific capacitance of the asymmetric supercapacitor is much higher than that of the EDLC. Even though under the large current density of 1666.7 mA/g, nearly 65.2% of the initial amount can be reached for the hybrid capacitor, so the large specific energy and well rate capability of the asymmetric capacitor makes it attractive, particularly for a practical application.

High power and energy densities are always objects for supercapacitor to pursue. Therefore, we also evaluate the relation between power and energy densities of the asymmetric supercapacitor and the EDLC. The values of power and energy densities are calculated from Eq. 3 and 4, respectively, and are depicted in Fig. 8. The data clearly demonstrated that the asymmetric supercapacitor based on AC and  $\text{Co}_{0.56}\text{Ni}_{0.44}$  oxide has a good specific energy and power density. For example, the specific energy was  $34.5 \text{ W h/kg}$  at a power density of  $133.3 \text{ W/kg}$  and still keeps  $22.5 \text{ W h/kg}$  at a power density of  $1333.3 \text{ W/kg}$ . Clearly both the energy density and power density greatly increased compared with the EDLC type. This can be explained by the energy and power densities, which critically depend on the real working voltage. The specific energy increases by more than eight times compared with that of a symmetric AC-based EDLC capacitor using an aqueous KOH electrolyte.

The cycling stability of the asymmetric supercapacitor was performed by charge–discharge at a current density of  $333.3 \text{ mA/g}$  within a voltage range of 0–1.6 V in the 2 M KOH electrolyte. As shown in Fig. 9, the capacitance of the hybrid supercapacitor decreases with the growth of the cycle number. After a continuous 1000 cycles, the capacitance value remains 83% of that of the first cycle. The attenuation of the capacitance just for 17% suggests the good stability of the  $\text{Co}_{0.56}\text{Ni}_{0.44}$  oxide/AC asymmetric supercapacitor, which is significant for the practical application.

### Conclusions

In summary,  $\text{Co}_{0.56}\text{Ni}_{0.44}$  oxide nanoflakes were successfully synthesized by a facile chemical coprecipitation method followed by

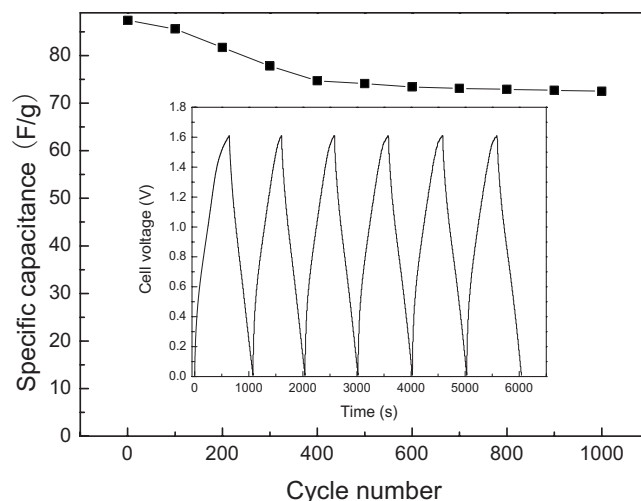


**Figure 9.** Cycle life of the asymmetric supercapacitor at the current density of  $333.3 \text{ mA/g}$ . The inset is charge/discharge curves of the asymmetric supercapacitor.

a simple calcinations process. The studies show that the as-prepared  $\text{Co}_{0.56}\text{Ni}_{0.44}$  oxide was composed of NiO and  $\text{Co}_3\text{O}_4$  with a less crystallization, nanoflake structure. The specific capacitance value of  $1227 \text{ F/g}$  ( $136 \text{ mAh/g}$ ) is obtained for the  $\text{Co}_{0.56}\text{Ni}_{0.44}$  oxide sample. Additionally, an asymmetric supercapacitor based on  $\text{Co}_{0.56}\text{Ni}_{0.44}$  oxide nanoflakes as the positive electrode and AC as the negative electrode with high operating voltage and high energy density was fabricated in the 2 M KOH electrolyte. The specific capacitance and specific energy of the cell reach  $97 \text{ F/g}$  and  $34.5 \text{ W h/kg}$  within the cell voltage range from 0 to 1.6 V, respectively. The hybrid supercapacitor also demonstrated a good cycling performance with an attenuation of capacitance of 17% over 1000 cycle numbers.

### Acknowledgments

This work was supported by the National Natural Science Foundation of China (grant no. 50602020) and the National Basic Research Program of China (grant no. 2007CB216408).

Lanzhou University of Technology assisted in meeting the publication costs of this article.

### References

1. M. Toupin, T. Brousse, and D. Bélanger, *Chem. Mater.*, **16**, 3184 (2004).
2. J. M. Ko, K. S. Ryu, S. Kim, and K. M. Kim, *J. Appl. Electrochem.*, **39**, 1331 (2009).
3. M. Winter and R. J. Brodd, *Chem. Rev.*, **104**, 4245 (2004).
4. A. Lewandowski and M. Galinski, *J. Power Sources*, **173**, 822 (2007).
5. T. Brousse, P. L. Taberna, O. Crosnier, R. Dugas, P. Guillemet, Y. Scudeller, Y. Zhou, F. Favier, D. Bélanger, and P. Simon, *J. Power Sources*, **173**, 633 (2007).
6. H. A. Mosqueda, O. Crosnier, L. Athouël, Y. Dandeville, Y. Scudeller, P. Guillemet, D. M. Schleich, and T. Brousse, *Electrochim. Acta*, In press. [DOI:]
7. N. W. Duffy, W. Baldsing, and A. G. Pandolfo, *Electrochim. Acta*, **54**, 535 (2008).
8. A. Burke, *Electrochim. Acta*, **53**, 1083 (2007).
9. Q. T. Qu, Y. Shi, S. Tian, Y. H. Chen, Y. P. Wu, and R. Holze, *J. Power Sources*, **194**, 1222 (2009).
10. J. H. Yoon, H. J. Bang, J. Prakash, and Y. K. Sun, *Mater. Chem. Phys.*, **110**, 222 (2008).
11. Z. Algharaibeh, X. R. Liu, and P. G. Pickup, *J. Power Sources*, **187**, 640 (2009).
12. K. H. An and W. S. Kim, *Adv. Funct. Mater.*, **11**, 387 (2001).
13. D. W. Wang, F. Li, M. Liu, G. Q. Lu, and H. M. Cheng, *Angew. Chem., Int. Ed.*, **47**, 373 (2008).
14. V. L. Pushparaj, M. M. Shaijumon, A. Kumar, S. Murugesan, L. Ci, R. Vajtai, R. J. Linhardt, O. Nalamasu, and P. M. Ajayan, *Proc. Natl. Acad. Sci. U.S.A.*, **104**, 13574 (2007).
15. J. Yan, T. Wei, B. Shao, F. Ma, Z. J. Fan, M. L. Zhang, C. Zheng, Y. C. Shang, W. Z. Qian, and F. Wei, *Carbon*, **48**, 1731 (2010).
16. L. Cao, F. Xu, Y. Y. Liang, and H. L. Li, *Adv. Mater.*, **16**, 1853 (2004).
17. Y. F. Ke, D. S. Tsai, and Y. S. Huang, *J. Mater. Chem.*, **15**, 2122 (2005).
18. T. Brezesinski, J. Wang, S. H. Tolbert, and B. Dunn, *Nature Mater.*, **9**, 146 (2010).
19. D. H. Wang, R. Kou, D. Choi, Z. G. Yang, Z. M. Nie, J. Li, L. V. Saraf, D. H. Hu, J. G. Zhang, G. L. Graff et al., *ACS Nano*, **4**, 1587 (2010).

20. Q. Wu, Y. X. Xu, Z. Y. Yao, A. R. Liu, and G. Q. Shi, *ACS Nano*, **4**, 1963 (2010).
21. J. Zhang, L. B. Kong, B. Wang, Y. C. Luo, and L. Kang, *Synth. Met.*, **159**, 260 (2009).
22. K. Zhang, L. L. Zhang, X. S. Zhao, and J. S. Wu, *Chem. Mater.*, **22**, 1392 (2010).
23. R. A. Huggins, *Solid State Ionics*, **134**, 179 (2000).
24. L. B. Kong, J. W. Lang, M. Liu, Y. C. Luo, and L. Kang, *J. Power Sources*, **194**, 1194 (2009).
25. J. W. Lang, L. B. Kong, W. J. Wu, M. Liu, Y. C. Luo, and L. Kang, *J. Solid State Electrochem.*, **13**, 333 (2009).
26. J. W. Lang, L. B. Kong, W. J. Wu, Y. C. Luo, and L. Kang, *Chem. Commun. (London)*, **35**, 4213 (2008).
27. L. Z. Fan, Y. S. Hu, J. Maier, P. Adelhelm, B. Smarsly, and M. Antonietti, *Adv. Funct. Mater.*, **17**, 3083 (2007).
28. W. C. Chen, T. C. Wen, and H. Teng, *Electrochim. Acta*, **48**, 641 (2003).
29. J. J. Deng, J. C. Deng, Z. L. Liu, H. R. Deng, and B. Liu, *J. Solid State Electrochem.*, **13**, 1387 (2009).
30. Z. R. Chang, H. J. Li, H. W. Tang, X. Z. Yuan, and H. J. Wang, *Int. J. Hydrogen Energy*, **34**, 2435 (2009).
31. V. Pralong, A. Delahaye-Vidal, B. Beaudoin, J. B. Leriche, and J. M. Tarascon, *J. Electrochem. Soc.*, **147**, 1306 (2000).
32. M. Oshitani, H. Yufu, K. Takashima, S. Tsuji, and Y. Matsumoru, *J. Electrochem. Soc.*, **136**, 1590 (1989).
33. J. H. Park, S. Kim, O. O. Park, and J. M. Ko, *Appl. Phys. A: Mater. Sci. Process.*, **82**, 593 (2006).
34. Z. R. Chang, Y. J. Zhao, and Y. C. Ding, *J. Power Sources*, **77**, 69 (1999).
35. M. Vidotti, M. R. Silva, R. P. Salvador, S. L. Córdoba de Torresi, and L. H. Dall'Antonia, *Electrochim. Acta*, **53**, 4030 (2008).
36. X. F. Wang, D. B. Ruan, and Z. You, *Trans. Nonferrous Met. Soc. China*, **16**, 1129 (2006).
37. L. Cao, M. Lu, and H. L. Li, *J. Electrochem. Soc.*, **152**, A871 (2005).
38. R. Kötz and M. Carlen, *Electrochim. Acta*, **45**, 2483 (2000).